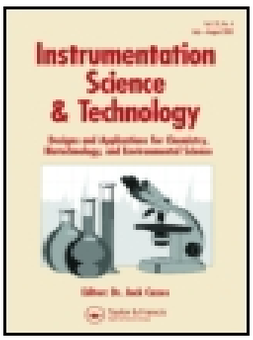

Instrumentation Science & Technology

ISSN: 1073-9149 (Print) 1525-6030 (Online) Journal homepage: https://www.tandfonline.com/loi/list20

Characterization of the influence of the fiber diameter and sensing region length upon lossy mode resonance (LMR) fiber sensors

Zhi-Wei Song, Qi Wang & Xue-Zhou Wang

To cite this article: Zhi-Wei Song, Qi Wang & Xue-Zhou Wang (2019): Characterization of the influence of the fiber diameter and sensing region length upon lossy mode resonance (LMR) fiber sensors, Instrumentation Science & Technology, DOI: 10.1080/10739149.2019.1636064

To link to this article: https://doi.org/10.1080/10739149.2019.1636064

Published online: 03 Jul 2019.

INSTRUMENTATION SCIENCE & TECHNOLOGY
https://doi.org/10.1080/10739149.2019.1636064

Taylor & Francis
Taylor & Francis Group

Characterization of the influence of the fiber diameter and sensing region length upon lossy mode resonance (LMR) fiber sensors

Zhi-Wei Song, Qi Wang, and Xue-Zhou Wang

College of Information Science and Engineering, Northeastern University, Shenyang, China

ABSTRACT

This paper explores high sensitivity fiber optic sensors based on lossy mode resonance (LMR). The sensitivity enhancement is achieved by simultaneously optimizing the diameter of the fiber core and the length of sensing region. The influence of these factors on the sensor sensitivity was analyzed by simulation using the transfer matrix method (TMM) and verified by experiments. The simulation results show that the sensor has high sensitivity and a narrow full width at half maxima when the sensing area is 10 mm. The sensitivity was as high as 3261 nm/refractive index units (RIU) when the core diameter is 200 μm. The experimental results have the same trend as the simulations, with a maximum value of 3100 nm/RIU. The resolution of the sensor may be as high as 1.29×10^{-8} RIU using a spectrometer with a resolution of 0.04 pm. The sensor was also shown to be relatively precise and stable. Since no systematic study concerning the influence of combining the sensing area length and fiber diameter on the sensor performance index yet has been published, this paper provides a reference for future characterization of high-sensitivity and high-precision optical fiber LMR sensors.

KEYWORDS

Lossy mode resonance (LMR); transfer matrix method (TMM); high sensitivity; fiber core diameter; sensing area length

Introduction

As an essential optical property of substances, the refractive index is widely characterized in the study of materials. In recent years, optical fiber sensors have attracted attention in liquid refractive index detection, using mode interference, fiber gratings, and surface plasmon resonance. The mode interference sensor uses interference between the modules, which couple a portion of the light transmitted by the fiber core mode into the cladding mode. After a specific transmission distance, the two modes produce a certain optical path, and interference occurs between the modes when the two modes are coupled again. The change of external refractive index influences the magnitude of optical path difference, thus causing the interference

CONTACT Qi Wang wangqi@ise.neu.edu.cn
Color versions of one or more of the figures in the article can be found online at www.tandfonline.com/list.

trough to move. However, this method of measurement significantly reduces the mechanical strength of the sensor.

The optical fiber grating refractive index sensors include two types: the fiber Bragg grating (FBG) and long-period grating (LPG). The fiber Bragg grating is insensitive to the refractive index of external liquid, so the grid area may directly contact the liquid by changing the structure of grating by corrosion cladding, molten pull cone, and single-side polishing. However, due to the low sensitivity of the fiber Bragg grating, it is difficult to measure subtle refractive index changes in chemical and biological analysis. [1]

Surface plasmon resonance is based on the phenomenon of a surface plasmon wave induced by a light wave deposited on the metal film of optical fiber core.[2] The surface plasma wave is a free electron wave localized on the metal surface, whose wave vector contains the refractive index of the medium to be measured. Therefore, the liquid refractive index may be measured by using this phenomenon. However, the surface plasmon resonant fiber sensor has several disadvantages.[3] For example, only the transverse magnetic wave stimulates the surface plasmon resonance effect, which not only reduces the utilization of light source, but also reduces the resolution of the sensor.

Lossy mode resonance (LMR) is a new optical sensing technology with rapid development in recent years.[4] It is extremely sensitive to small changes in the refractive index of external media. Its combination with optical fiber sensing technology greatly improves the sensitivity and resolution of the device. This approach also offers many advantages over traditional mechanical and electrical sensors, such as sensor microform, online measurements, and biological identification functions,[5] Consequently, lossy mode resonance has been employed in biology, medical pharmacy, chemistry, petrochemical industry, environmental monitoring, and food detection.[6–16]

In 2010, Zamarreno proposed an optical fiber humidity sensor based on LMR.[17] The surface of the humidity sensor was coated with indium tin oxide/polycyclic aromatic hydrocarbon/polyacrylic acid. The indium tin oxide was used to generate LMR and the polycyclic aromatic hydrocarbon/polyacrylic acid was employed to determine the humidity. The sensitivity of this humidity sensor was shown to reach 5.4 relative humidity%/nm.

In 2012, Socorro applied polycyclic aromatic hydrocarbon/sodium-p-styrenesulfonate coated multimode optical fibers for the monitoring of biological reactions.[18–22] Polycyclic aromatic hydrocarbon/sodium-p-styrenesulfonate produced LMR and provided a suitable substrate for the combination of immunoglobulin G and anti-immunoglobulin G. The measurements showed that the wavelength changed by 10 nm at an immunoglobulin G concentration of 50 μg/ml.

In 2013, Elosua used a multimode optical fiber coated with an organometallic compound $(Au_2Ag_2(C_6F_5)_4(C_6H_5C{\equiv}CC_6H5)_2]_n$ to determine volatile organic compounds.[19] The sensitivity response values to ethanol, methanol and isopropanol were 0.417 nm/ppm, 0.520 nm/ppm and 263 nm/ppm, respectively.

In 2014, Socorro used an LMR-based conical fiber optic sensor to detect celiac disease.[23] In order to develop high-precision and high-sensitivity sensors, optical fibers and thin film structures were explored in depth. Del Villar proposed a liquid refractive index sensor coated with indium tin oxide using the LMR effect in 2010.[24] The sensitivity value was as high as 2952 nm/RIU.

In the same year, Paliwal conducted a simulation study on the LMR refractive index sensor coated with indium tin oxide/titanium dioxide.[25] The results showed that the sensitivity of the LMR refractometer coated with indium tin oxide/titanium dioxide material was several times higher than for the LMR refractometer coated with titanium dioxide.

In 2015, Socorro reported a D-shaped multimode fiber optic liquid refractive index sensor coated with indium tin oxide,[26] which has high sensitivity, a 6.9 nm resonance bandwidth, and a 36 dB resonance depth. Zubiate reported the use of a conical single-mode fiber in an LMR refractometer.[27] Compared with multi-mode fibers, this device is more compact and has higher sensitivity. The bandwidth of the resonance valley was narrowed and the resonance depth increased, which enhanced the sensitivity and improved the resolution.

In 2010, Del Villar studied the influence of indium tin oxide and indium oxide films on the performance of LMR sensors in multimode fibers.[28] The results showed that the sensitivity obtained with indium tin oxide coated devices was improved by more than a factor of two compared to the In_2O_3 coated devices.

In 2014, Paliwal and coworkers conducted in-depth characterization of the combination of different types of multimode optical fiber films.[25] He showed that there was almost a two fold increase in the sensitivity using the indium tin oxide/titanium dioxide bilayer combination compared to a single indium tin oxide layer employing the same total thin film thickness. Hernaez et al. [29] used titanium dioxide/sodium-p-styrenesulfonate films to explore the effect of film thickness on LMR excitation. The results showed that when the coating is thicker, an absorption peak was created at low wavelengths, which was shifted to higher wavelengths as the coating thickness increased. Subsequently, new peaks appeared at low wavelengths and follow the same pattern as the first LMR.

In 2017, Paliwal and colleagues used a multi-mode optical fiber to explore the influence of different numerical aperture sizes on the excitation

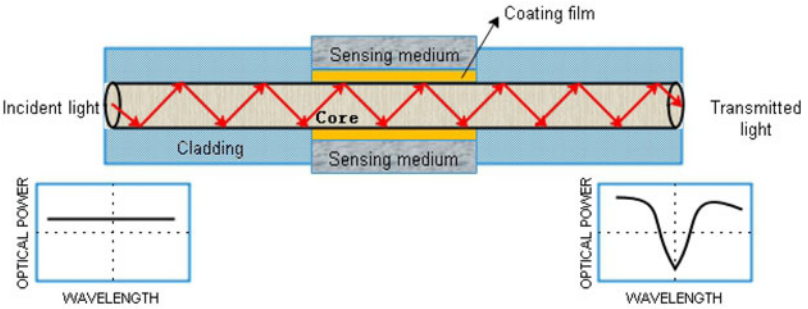

Figure 1. Structure of the three-layer fiber waveguide.

LMR phenomena.[30] The authors concluded that from 0.22 to 0.42, the larger the numerical aperture, the narrower the excitation resonance trough. In order to optimize the structure of the sensor and explore the excellent sensing properties, the fiber structure, film material and film thickness were varied. However, no systematic study concerning the influence of combining the sensing area length and fiber diameter on the sensor performance index yet has been published.[31] There is therefore a need, although a significant challenge, to explore these parameters in detail.

In this paper, a high sensitivity fiber optic sensor based on lossy mode resonance (LMR) is reported. The sensitivity of the sensor was improved by optimizing the diameter of the optical fiber core and the length of the sensing region. The influence of these two parameters on the sensitivity of the sensor were analyzed theoretically and subsequently verified experimentally. The simulation and experimental results correspond well, as the maximum sensitivity values were 3261 nm/RIU and 3100 nm/RIU, respectively. The stability of the sensor was evaluated and the results show that the device has suitable characteristics for practical measurements.

Principles of lossy mode resonance

The principles of lossy mode resonance (LMR) are shown in Figure 1. The generation of LMR is essentially due to the coupling between the core and the film coating modes. When the phase matching condition and the mode overlap are satisfied, the energy in the core leaks into the coating film with high refractive index and eventually become a mode in the film. Therefore, when the resonance condition is satisfied for LMR, one or more attenuations are formed in the spectrum. When the refractive index of the sensing medium changes, the effective refractive index of light propagating in the thin film also varies, thus leading to a change in the resonance wavelength. Therefore, the refractive index of the sensing medium may be determined by monitoring the variation in the resonance wavelength.

In order to optimize the sensor structure, a narrow half-peak full width and high sensitivity were evaluated using a simulation by the transfer matrix method (TMM) using Matlab software. TMM uses Maxwell 's equations to solve the electric field and magnetic field on two adjacent layers in order to obtain the transmission matrix. The results of the single layer are extended to the entire medium to determine the transmission and reflection coefficients. This approach is suitable for the simulation of the large core diameter multi-mode fiber with a rapid calculation speed. First, a three-layer waveguide mathematical model based on the multi-mode fiber was constructed.

Figure 1 shows that if an optical fiber surface is coated with a layer of sensing film, the coating area may be considered to be a composite waveguide composed of three layers of waveguides, fiber core, coating film and sensing medium. Light waves propagate in the three layers of waveguides. The transmitted light is reflected from the incident radiation on the composite waveguide. According to Fresnel's law of reflection, reflectivity and light output power may be described by:

$$\mathrm{p}(\theta,\lambda) \propto k_0^2(\lambda) n_{core}^2(\lambda) \sin\theta\cos\theta \tag{1}$$

where n_{core} is the refractive index of the fiber core; θ is the incident angle; p is the light power; and k_0 is the wavenumber. The wavenumber values and refractive index of the fiber core may be evaluated by:

$$k_0(\lambda) = \frac{2\pi}{\lambda} \tag{2}$$

$$n_{core}(\lambda) = \sqrt{1 + \frac{a_1\lambda^2}{\lambda^2 - {b_1}^2} + \frac{a_2\lambda^2}{\lambda^2 - {b_2}^2} + \frac{a_3\lambda^2}{\lambda^2 - {b_3}^2}} \tag{3}$$

The multimode fiber has multiple modes, so the incident angle ranges from the critical angle to 90°. In addition, the light may be tilted into the optical fiber end face, so the normalized power of transmitted light is described by:

$$P_{trans}(\lambda) = \frac{\int_0^{\alpha max}\int_{\theta_c}^{\frac{\pi}{2}} R^{N_{ref}(\theta,\alpha)}(\theta,\lambda) p(\theta,\lambda)\mathrm{d}\theta\mathrm{d}\alpha}{\int_0^{\alpha max}\int_{\theta_c}^{\frac{\pi}{2}} p(\theta,\lambda)\mathrm{d}\theta\mathrm{d}\alpha} \tag{4}$$

where N_{ref} is the reflection frequency of light wave in the coating area, which is related to the length L of the sensing area, the fiber diameter D, incidence angle and inclination angle of the light. This relationship is given by:

$$N_{ref}(\theta,\alpha) = \frac{L}{D\tan\theta\cos\alpha} \tag{5}$$

For unpolarized light, transverse electric and transverse magnetic modes are considered, so the total reflectance is the sum of their respective

reflectance values. This relationhip is

$$R^{N_{ref}(\theta,\alpha)}(\theta,\lambda) = \frac{R_{TM}^{N_{ref}(\theta,\alpha)}(\theta,\lambda) + R_{TE}^{N_{ref}(\theta,\alpha)}(\theta,\lambda)}{2} \tag{6}$$

The formulas for the reflectivity of transverse magnetic and transverse electric modes are given by:

$$R_{TM}(\theta,\lambda) = \left| \frac{r_{st}^{TM} + r_{td}^{TM} e^{(2ik_{tz}q)}}{1 + r_{st}^{TM} r_{td}^{TM} e^{(2ik_{tz}q)}} \right|^2 \tag{7}$$

$$R_{TE}(\theta,\lambda) = \left| \frac{r_{st}^{TE} + r_{td}^{TE} e^{(2ik_{tz}q)}}{1 + r_{st}^{TE} r_{td}^{TE} e^{(2ik_{tz}q)}} \right|^2 \tag{8}$$

The dielectric constant of titanium dioxide is described by the Lorentz model:

$$\varepsilon(E) = \sum\nolimits_k \frac{A_K}{E_k^2 - E^2 - iB_k E} + \varepsilon_\infty \tag{9}$$

$$n_{TiO_2} = \varepsilon^2(E) \tag{10}$$

where A_k represents the amplitude, B_k refers to the center energy, E is the photon energy, $\varepsilon(E)$ is the dielectric constant of titanium dioxide, n_{TiO2} is the refractive index of titanium dioxide, and ε_∞ is the high frequency dielectric constant. The single oscillator model, which is used for the simplicity, has given the best fit parameters for the simulation, which are described below:

$$\varepsilon_\infty = 1, \quad B_k = 1.2\text{eV}, \quad A_k = 101\text{eV}^2, \quad \text{and} \quad E_k = 6.2\text{eV}$$

Simulations and analysis

Based on the mathematical model of the multi-mode fiber LMR effect, a transfer matrix method (TMM) simulation was used to explore the influence of fiber sensing length and fiber core diameter on the sensor performance. The diameters of fiber core were 100 μm, 200 μm, and 600 μm. The lengths of the sensing area were 5, 10, 15, and 20 mm. A 80 nm titanium dioxide coating was employed.

Simulation results

Simulation analysis of the LMR sensor using 100 μm optical fibers

Figure 2 shows the transmission spectra and sensitivity fit when the lengths of the sensing area were 5, 10, 15 and 20 mm using 100 μm optical fibers.

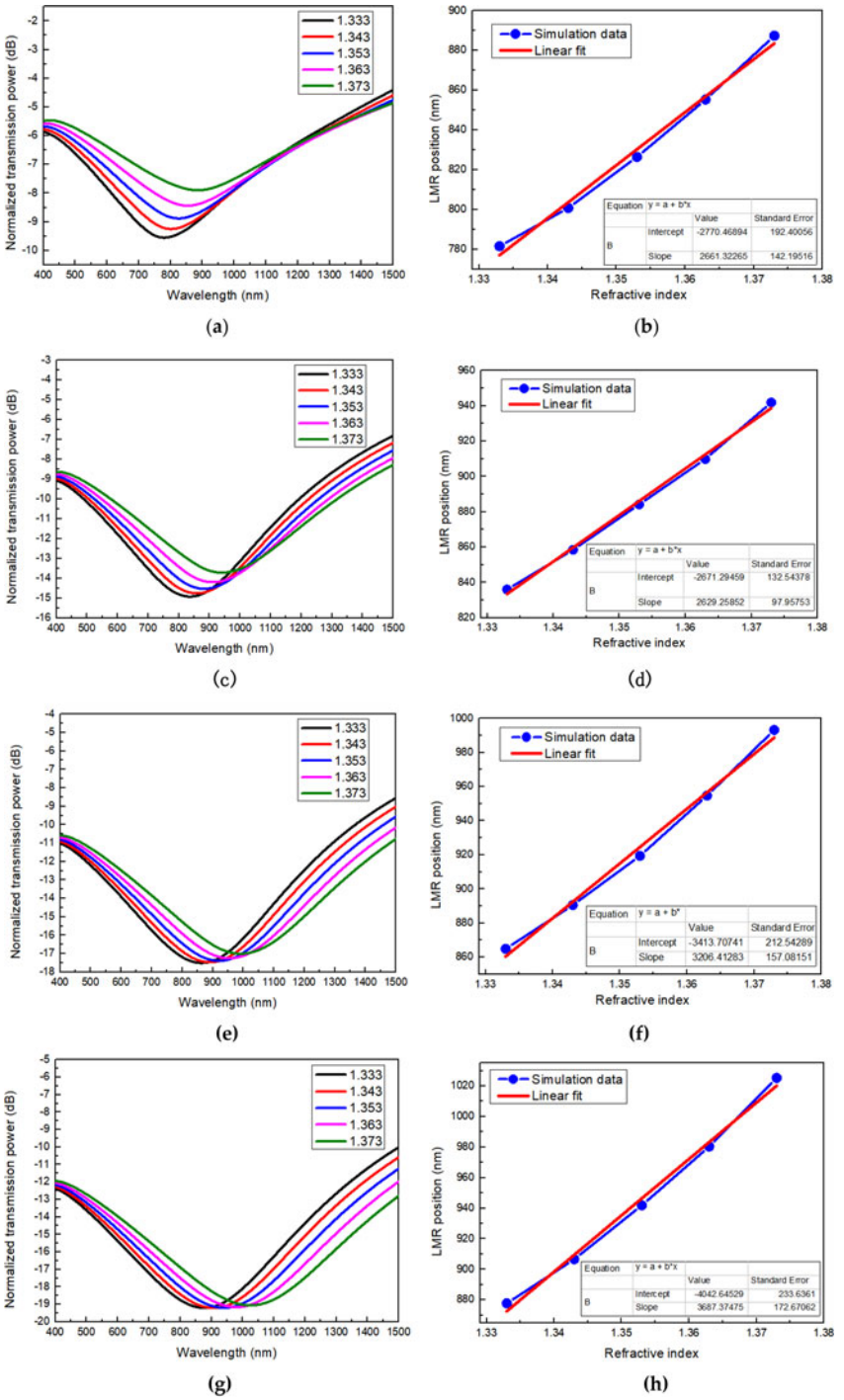

Figure 2. Simulation results of the 100 μm optical fiber: (a) Transmission spectrum when the length of the sensing region is 5 mm. (b) Sensitivity fitting diagram when the length of the sensing region is 5 mm. (c) Transmission spectrum when the length of the sensing region is10 mm. (d) Sensitivity fitting diagram when the length of the sensing region is10 mm. (e) Transmission spectrum when the length of the sensing region is 15 mm. (f) Sensitivity fitting diagram when the length of the sensing region is 15 mm. (g) Transmission spectrum when the length of the sensing region is 20 mm. (h) Sensitivity fitting diagram when the length of the sensing region is 20 mm.

The transmission spectrum was detected across the refractive index range from 1.333 to 1.373.

The results show that with the increase of the refractive index of the external environment, the LMR resonance trough gradually moves to the right, the optical wave losses decrease, and the resonance trough moves up. According to sensitivity fitting measurements in Figure 2, when the lengths of sensing region were 5, 10, 15, and 20 mm, the corresponding sensitivity values were 2661, 2629, 3206, and 3687 nm/RIU, respectively. The sensitivity generally increased with the length of the sensing region. Figure 2 shows that when the sensing area was 15 and 20 mm, a wide full width at half maximum was obtained.

Simulation analysis of the LMR sensor using 200 μm optical fibers

Figure 3 shows the transmission spectra and sensitivity fit diagram of the optical fiber at the sensing region lengths of 5, 10, 15, and 20 mm using 200 μm optical fibers. With an increase in the refractive index, the LMR resonance trough moves to the right, the optical wave loss decreases, and the trough moves up. When the lengths of sensing area were 5, 10, 15 and 20 mm, the sensitivity values obtained by the simulation were 2436, 2961, 2565, and 2629 nm/RIU, respectively. The maximum sensitivity was observed when the length of the sensing region was 10 mm. A wider full width at half maximum of the waveform was obtained with increases in the refractive index of the measured solution. Using the same refractive index, the full width at half maximum did not vary significantly with the sensing region length.

Simulation analysis of the LMR sensor using 600 μm optical fibers

Figure 4 shows the transmission spectrum and sensitivity fitting diagram of optical fiber at the sensing region lengths of 5, 10, 15 and 20 mm using 600 μm optical fibers. As the external concentration increases, the resonance trough moves to the right, the optical losses decrease, and the trough moves up. Using the sensitivity fitting diagrams in Figure 4, when the sensing area lengths were 5, 10, 15 and 20 mm, the sensitivity values obtained by simulation were 1635, 2180, 2436 and 2565 nm/RIU, respectively. Hence, with an increase in the sensing area, the sensitivity of the device is slightly increased.

Simulation analysis

Figure 5a shows the sensitivity of fibers with diameters of 100, 200 and 600 μm using 5, 10, 15 and 20 mm sensing region lengths. Figure 5b shows

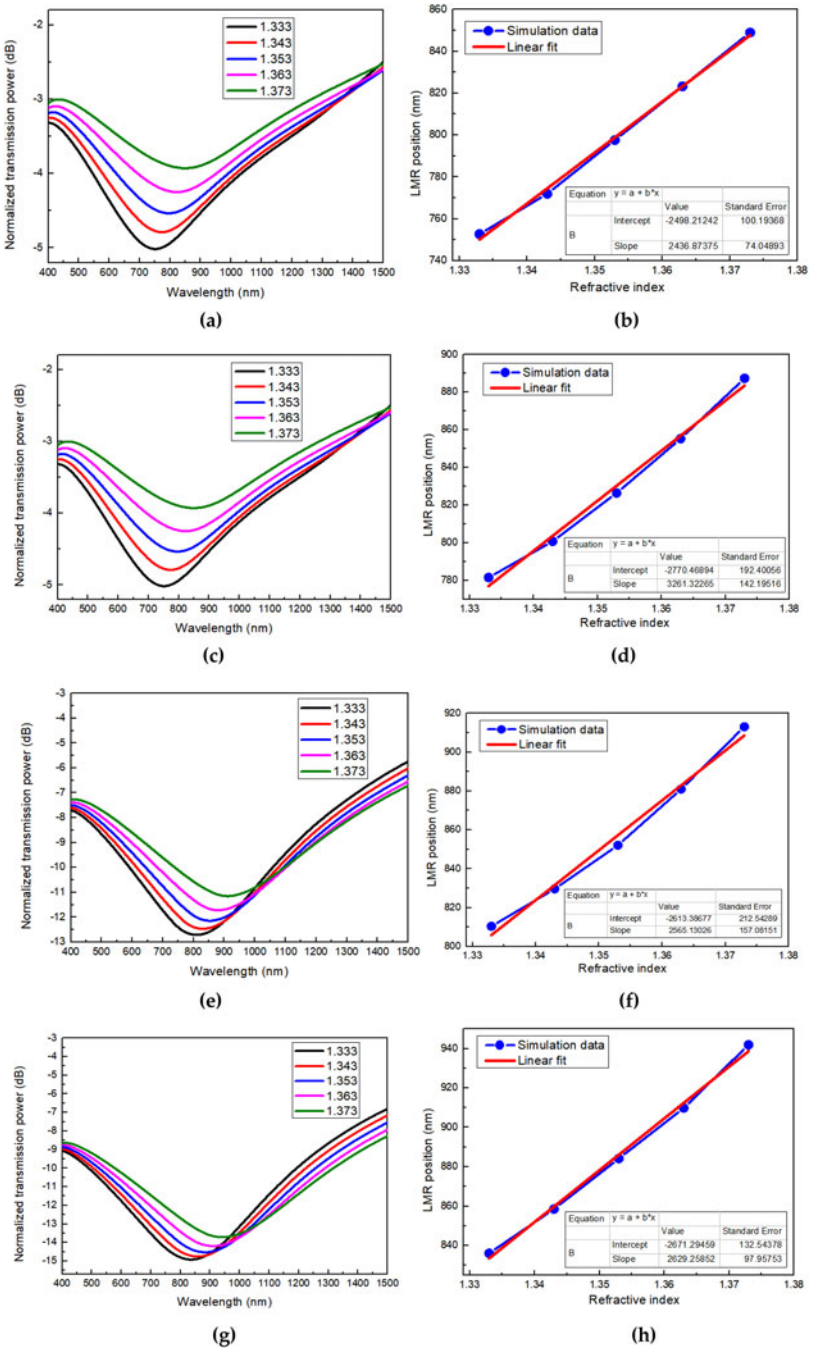

Figure 3. Simulation results of the 200 μm optical fiber. (a) Transmission spectrum when the length of the sensing region is 5 mm. (b) Sensitivity fitting diagram when the length of the sensing region is 5 mm. (c) Transmission spectrum when the length of the sensing region is 10 mm. (d) Sensitivity fitting diagram when the length of the sensing region is 10 mm. (e) Transmission spectrum when the length of the sensing region is 15 mm. (f) Sensitivity fitting diagram when the length of the sensing region is 15 mm. (g) Transmission spectrum when the length of the sensing region is 20 mm. (h) Sensitivity fitting diagram when the length of the sensing region is 20 mm.

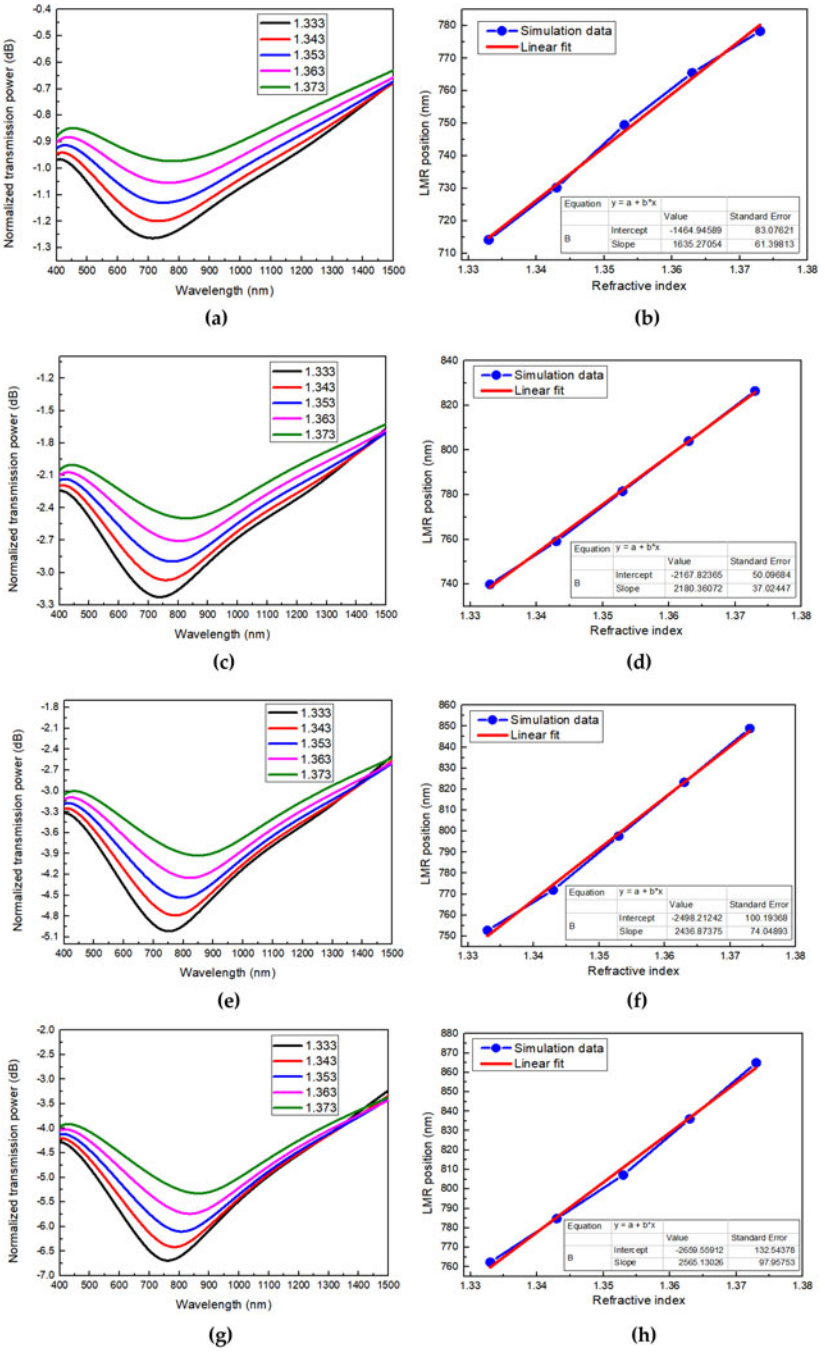

Figure 4. Simulation results of the 600 μm optical fiber. (a) Transmission spectrum when the length of the sensing region is 5 mm. (b) Sensitivity fitting diagram when the length of the sensing region is 5 mm. (c) Transmission spectrum when the length of the sensing region is 10 mm. (d) Sensitivity fitting diagram when the length of the sensing region is 10 mm. (e) Transmission spectrum when the length of the sensing region is 15 mm. (f) Sensitivity fitting diagram when the length of the sensing region is 15 mm. (g) Transmission spectrum when the length of sensing region is 20 mm. (h) Sensitivity fitting diagram when the length of the sensing region is 20 mm.

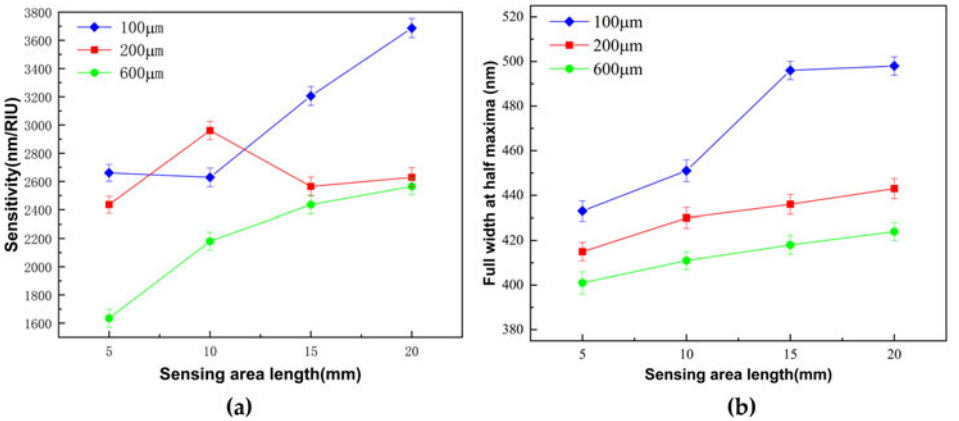

Figure 5. Simulation results of the 100, 200 and 600 μm fibers as a function of the sensing region length: (a) sensitivity comparison and (b) comparison of the full width at half maximum.

the full width at half maxima of the transmission spectrum measured when the refractive index of the external solution is equal to 1.333. The results show that the sensitivity of optical fibers with core diameters of 100 and 200 μm provided an increase with the sensing region length. However, the sensitivity of optical fibers with core diameters of 200 μm have a maximum value of 2961 nm/RIU using a sensing area region of 10 mm.

Figure 5b shows that with an increase in the sensing region length, the full width at half maximum of the transmission spectrum slightly increases. However, the value for the optical fiber with a core diameter of 100 μm dramatically increases to 496 nm using a sensing region length of 15 mm. Figure 5a shows that the optical fiber has high sensitivity values of 3206 and 3687 nm/RIU at sensing area lengths of 15 and 20 mm when the core diameter is 100 μm.

However, Figure 5b shows that the full width at half maximum is particularly large, which leads to a significant degradation in the accuracy. Moreover, the longer the sensing area, the more susceptible the optical fiber probe is to damage. Therefore, a fiber-optic probe with a core diameter of 200 μm and a sensing area length of 10 mm were deemed to be optimum. The sensitivity is as high as 2961 nm/RIU, second only to a diameter of 100 μm using sensing regions of 15 and 20 mm. In addition, this configuration also provides a narrow full width at half maxima.

By changing the structural parameters such as the diameter of the fiber core and the length of the sensing region, the distribution and number of modes of light in the fiber core were changed, thereby affecting the coupling between the fiber core and the film. Accordingly, the order of guided modes in the sensing film is changed. The change of mode field distribution corresponds to the variation of the sensitivity. The number of modes corresponds to the changes in the full width at half maxima. Therefore, the

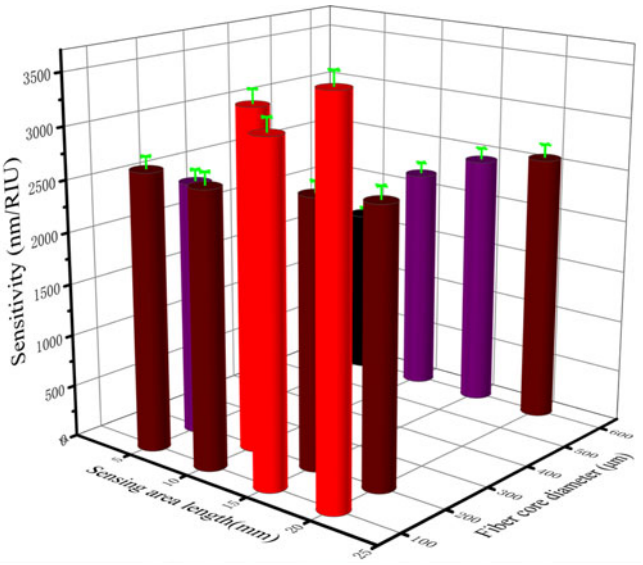

Figure 6. Influence of the 100, 200 and 600 μm fibers on sensor sensitivity as a function of sensing region length and fiber core diameter.

sensitivity and full width at half maxima of the sensor are varied by changing the length and diameter of the sensing region of the fiber core.

Figure 6 shows that for a fixed core diameter, the change in the sensitivity with the length of sensing region does not follow a single relationship. Some values change linearly with the length of the sensing region, while others followed a parabolic trend. These phenomena occurred because that the diameter of the optical fiber and the length of the sensing region have cross-influences on the sensor sensitivity and both affect the sensitivity.

Experimental results and analysis

Since the simulation results show high sensitivity and narrow half-peak full width using the 10 mm sensing region length, layer by layer self-assembly technology was employed to coat sodium-p-styrenesulfonate and titanium dioxide films of 80 nm thickness in order to characterize the sensitivity for 100, 200, 400, 600 and 1000 μm core diameters.

Reagents and apparatus

KOH solution (1 mol/L, Shanghai, China) was used to coat the initial fiber surface with negative ions. Sodium-p-styrenesulfonate solution (SigmaAldrich, St. Louis, MO, USA) and titanium dioxide solution (SigmaAldrich, St. Louis, MO, USA) were used to coat the optical fiber sensing region film. Acetone was employed to remove organic impurities from the surface of optical fibers (SigmaAldrich, St. Louis, MO, USA).

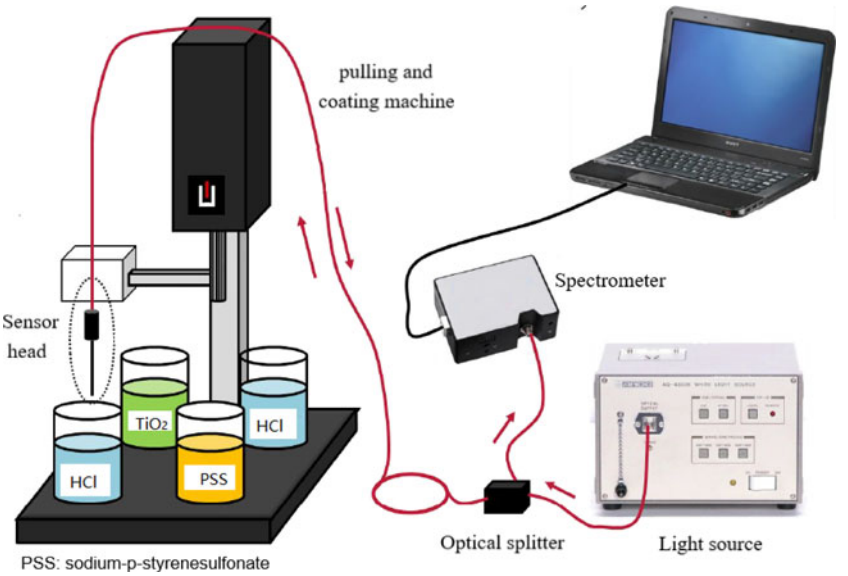

Figure 7. Experimental setup optimizing the diameter of the fiber core and the length of sensing region.

In order to completely remove the reagent residues, pH 2 acid purified water using 37.5% HCl was employed. All solutions are prepared using purified water (Shanghai, China).

All of the experiments were carried out in a temperature-controlled laboratory.

High purity nitrogen (Chengdu, China) was used to deoxidize and dry the optical fibers.

A pulling and coating machine (Sydc-100, Shanghai, China) was used for uniform and stable coating.

An optical splitter (Himing, Shanghai, China) transmitted the incident light to the sensing region and the reflected light to the spectrometer. The spectrometer used in this work is an Ap204xb (Apex, France), which has a measurement resolution of 0.04 pm. The light source Wl-sc-400-20 (Apex, France) is used to provide stable light with wavelengths ranging from 400 to 1500 nm.

100, 200 and 600 µm plastic-clad silica fibers were purchased from Beijing Scitlion Technology, with a numerical aperture of 0.37 and core cladding diameter ratios of 100/130, 200/230 and 600/630, respectively.

Experimental set-up

Conventional ultrasonic cleaning was performed first. The fiber core was placed into a beaker and treated with ultrasound in acetone for 10 minutes to remove grease and other organic impurities on the substrate. An

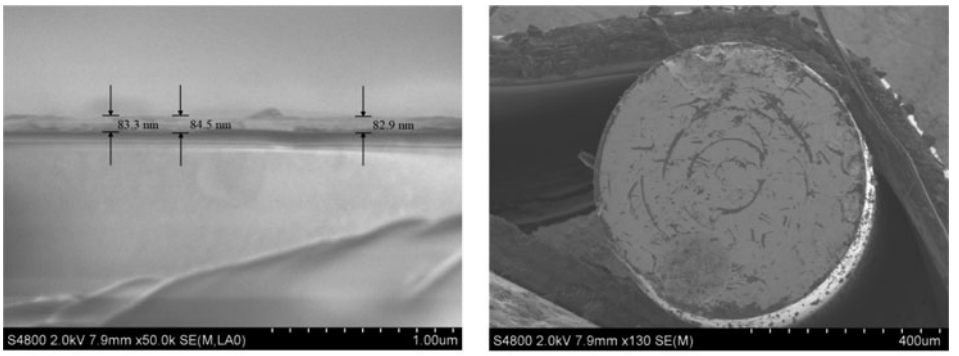

Figure 8. Images of the 600 μm fiber obtained by scanning electron microscopy following coating with titanium dioxide: (a) front view of the titanium dioxide film and (b) cross section of the fiber.

additional 10 minutes of ultrasound in anhydrous ethanol was employed to remove the acetone, followed by 10 minutes of ultrasound using deionized water to remove the anhydrous ethanol. The fiber was then dried with a stream of nitrogen.

The core was treated with ultrasound in KOH solution for 10 minutes in order to provide the surface of the core with a negative charge. Next, fiber was soaked in titanium dioxide solution for 5 minutes, rinsed with deionized water at pH 2 for 1 minute, and dried with a stream of nitrogen. The fiber was subsequently treated with sodium-p-styrenesulfonate solution for 5 minutes, rinsed with ionized water with a pH of 2 for 1 minute, and dried by a stream of nitrogen. This protocol was repeated until the core was ready for use.

Figure 7 shows a schematic diagram of the experimental setup. The light emitted from the light source is transmitted to the sensing region by the optical splitter. After the resonance between the light wave and the object is measured, the reflected light is transmitted to the spectrometer by the optical splitter. Due to the lossy mode resonance at a specific wavelength of the incident light wave, a resonance trough is formed in the spectrometer.

Figure 8 shows scanning electron micrograph of a fiber with a core diameter of 600 μm and a numerical aperture of 0.37. Three spots were selected to measure the thickness of titanium dioxide thin film, with values of 83.3 nm, 84.5 nm and 82.9 nm. The results in Figure 8 demonstrate that the thin film is relatively uniform.

Experimental results and analysis

Figure 9 shows that, with an increase of the refractive index of the object to be measured, the resonance trough moves to the right, the optical wave

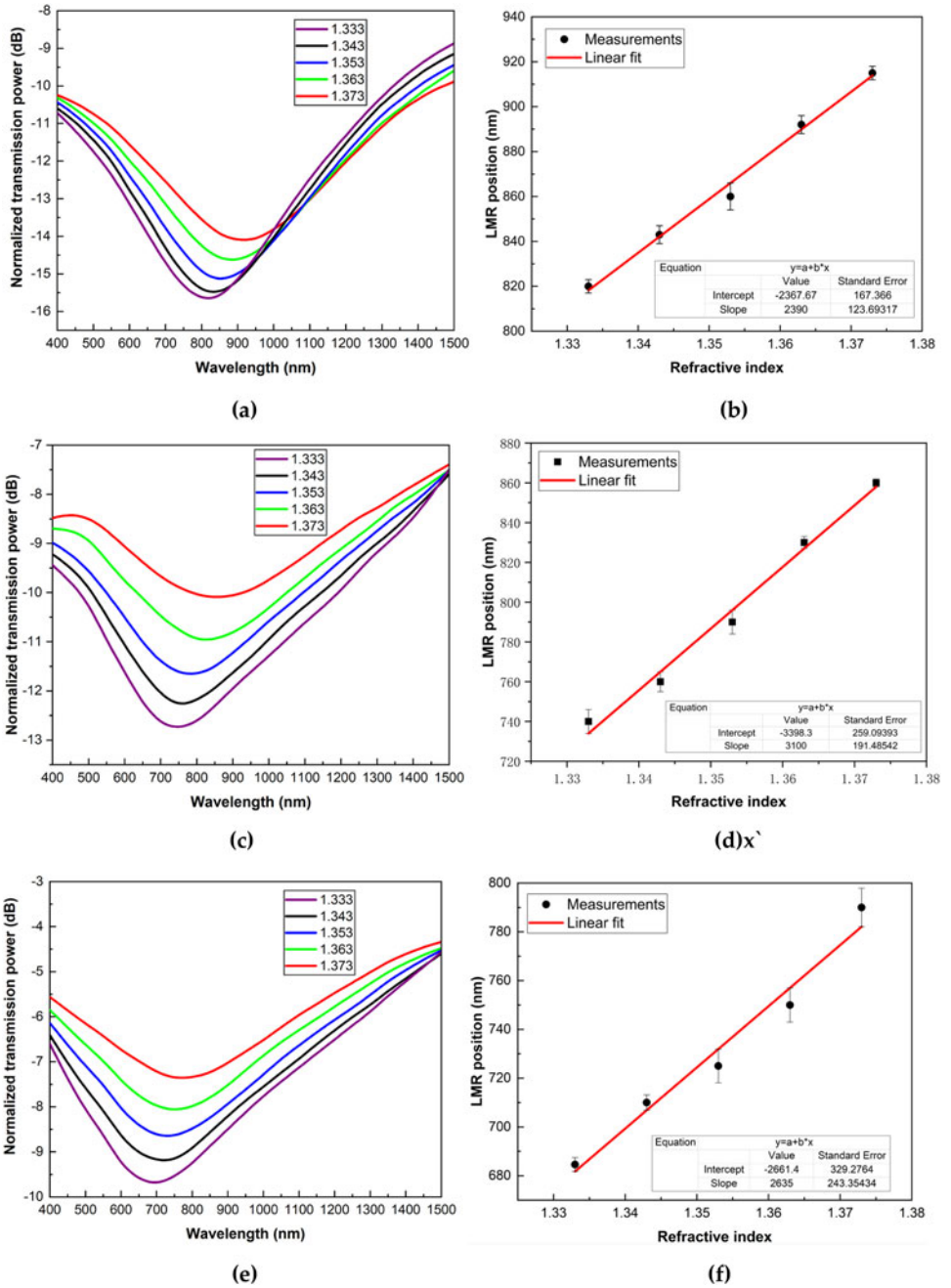

Figure 9. Optical fiber experimental results when the sensing area is 10 mm. (a) Optical fiber LMR transmission spectra using a 100 μm diameter. (b) Sensitivity fitting diagram using a 100 μm diameter. (c) Optical fiber LMR transmission spectra using a 200 μm diameter. (d) Sensitivity fitting diagram using a 200 μm diameter. (e) Optical fiber LMR transmission spectra using a 400 μm diameter. (f) Sensitivity fitting diagram using a 400 μm diameter. (g) Optical fiber LMR transmission spectra using a 600 μm diameter. (h) Sensitivity fitting diagram using a 600 μm diameter. (i) Optical fiber LMR transmission spectra using a 1000 μm diameter. (j) Sensitivity fitting diagram using a 1000 μm diameter.

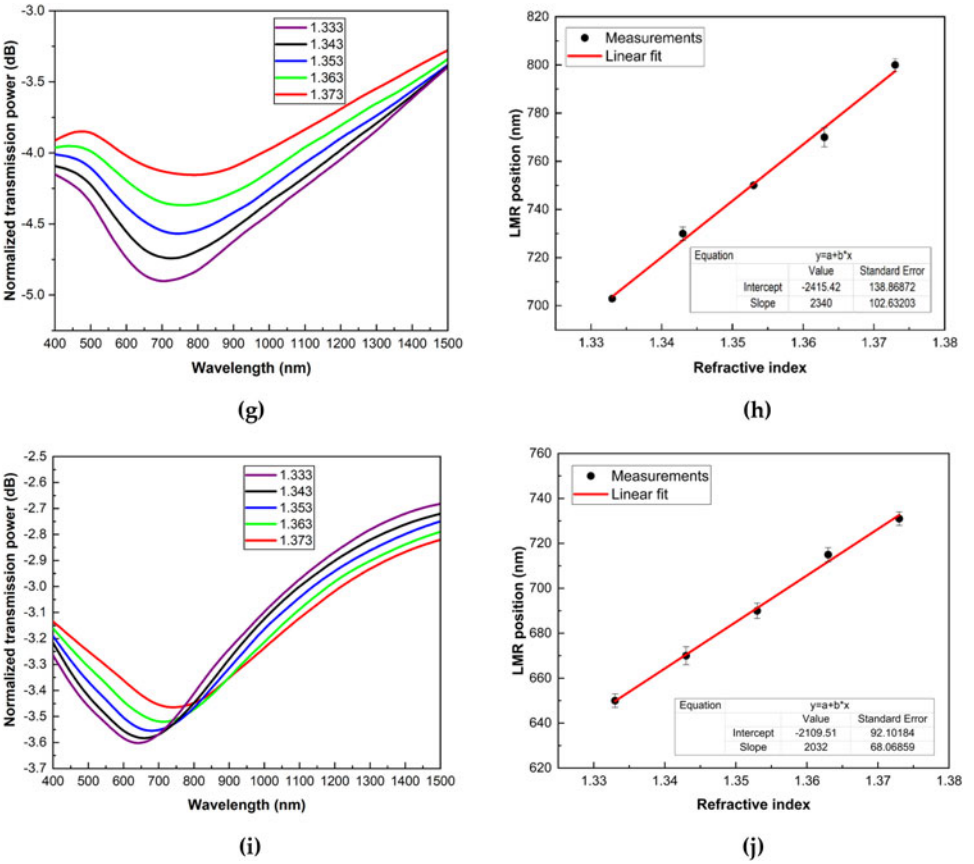

Figure 9. Continued.

loss increases, and the resonance trough becomes deeper. These observations are consistent with the simulation results. However, the transmission spectral losses are slightly larger than for the simulation results because of losses in the reflected light in the experiments, and therefore the projection loss curve is shifted downwards.

Figure 10 shows that the experimental results are basically consistent with the simulation results. The maximum sensitivity is at a 200 μm diameter, followed by 400 μm and 100 μm. The simulation sensitivity is higher than the experimental sensitivity at 100 μm, 200 μm and 400 μm diameters, while the experimental sensitivity is higher at 600 μm and 1000 μm diameters. This phenomenon occurs because in the experiments, the light wave propagation and reflection at the sensor probe have losses that are not considered in the simulation. In order to further improve the experimental measurements, optical fibers with lower transmission losses should be employed and the optical fiber probe port should be coated with a more compact reflection film to reduce these processes.

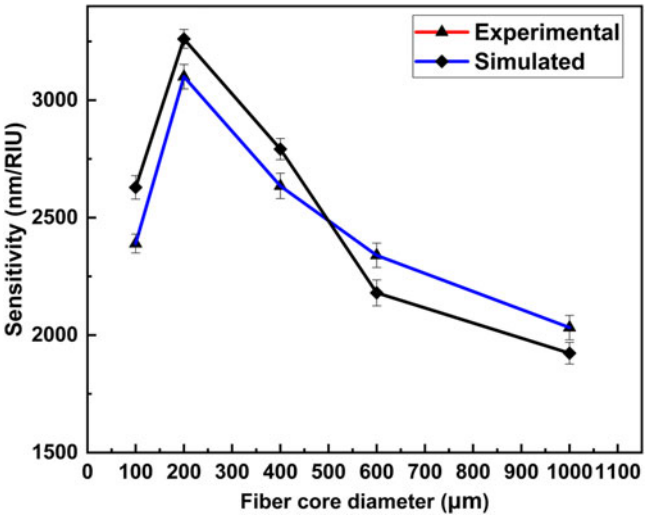

Figure 10. Comparison of the experimental and simulation sensitivity results.

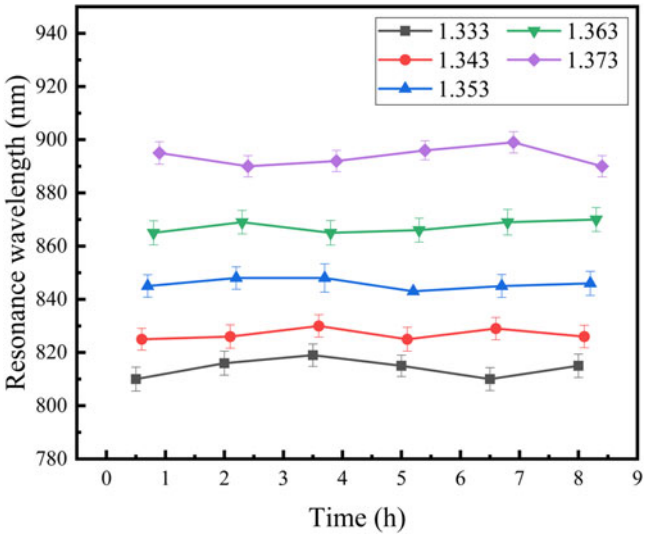

Figure 11. Characterization of the stability and precision of the optical fiber sensor.

Sensor reliability

There is no doubt that the reproducibility and stability of the optical device are necessary parameters to characterize for practical applications. In order to verify the stability and precision of the optical fiber sensor, a device with a sensing area length of 10 mm, a fiber diameter of 100 μm, and a film thickness of 80 nm was employed to make replicate measurements of one solution across an eight hour period.

Figure 11 shows a total of six measurements were performed, each separated by a time interval of one-and-a-half hours. Five measurements were

performed at each time interval. In order to ensure the accuracy of the measurements, the fiber optic sensor was rinsed with deionized water and dried with nitrogen following each measurement. The standard deviation values of the six measurements were evaluated and the results are shown in Figure 11, demonstrating that the fiber optic sensor has suitable stability and precision for practical measurements.

Conclusions

A high sensitivity fiber optic sensor based on lossy mode resonance (LMR) has been reported. The sensitivity enhancement was achieved by simultaneously optimizing the diameter of the fiber core and the length of the sensing area. The influence of two factors on sensor sensitivity were characterized theoretically and verified by experiments by coating titanium dioxide/sodium-p-styrenesulfonate nanofilms on the core of cladding removed multimode fiber using the layer-by-layer method.

The simulation results show that the sensor has high sensitivity and a narrow half-peak full width when the sensing area is 10 mm. The sensitivity was as high as 3261 nm/RIU when the core diameter was 200 μm. The experimental results have the same trend as the sensitivity of the simulations. The maximum value reached 3100 nm/RIU, which matches the simulation results. The precision and stability of the sensor were characterized, and the results demonstrate values suitable for practical measurements. In future work, the experimental error may be reduced by coating the sensor probe port with a denser reflection film and selecting an optical fiber with lower transmission losses.

Disclosure statement

No potential conflict of interest reported by the authors.

Funding

This work was supported by the Fundamental Research Funds for the Central Universities by Grants N180402023 and N172002001 and the National Natural Science Foundation of China by Grant 51607028.

References

[1] Bekmurzayeva, A.; Dukenbayev, K.; Shaimerdenova, M.; Bekniyazov, I.; Ayupova, T.; Sypabekova, M.; Molardi, C.; Tosi, D. Etched Fiber Bragg Grating Biosensor Functionalized with Aptamers for Detection of Thrombin. *Sensors* **2018**, *18*, 4298. DOI: 10.3390/s18124298.

[2] Deng, S. J.; Wang, P.; Yu, X. L. Phase-Sensitive Surface Plasmon Resonance Sensors: Recent Progress and Future Prospects. *Sensors*. **2017**, *17*, 2819. DOI: 10.3390/s17122819.

[3] Jing, J. Y.; Wang, Q.; Zhao, W. M.; Wang, B. T. Long-Range Surface Plasmon Resonance and Its Sensing Applications: A Comprehensive Review. *Opt. Lasers Eng.* **2019**, *112*, 103–118. DOI: 10.1016/j.optlaseng.2018.09.013.

[4] Andreev, A.; Pantchev, B.; Danesh, P.; Zafirova, B.; Karakoleva, E.; Vlaikova, E.; Alipieva, E. A Refractometric Sensor Using Index-Sensitive Mode Resonance between Single-Mode Fiber and Thin Film Amorphous Silicon Waveguide. *Sens. Actuators B Chem* **2005**, *106*, 484–488. DOI: 10.1016/j.snb.2004.09.002.

[5] Wang, Q.; Zhao, W. M. A Comprehensive Review of Lossy Mode Resonance Based Fiber Optic Sensors. *Opt. Lasers Eng.* **2018**, *100*, 47–60. DOI: 10.1016/j.optlaseng.2017.07.009.

[6] Pedro, J.; Rivero, A.; Urrutia, J.; Goicoechea, I. R.; Matias, F. J.; Arregui, A. Lossy Mode Resonance Optical Sensor Using Silver Nanoparticles-Loaded Films for Monitoring Human Breathing. *Sensors Actuat. B: Chem.* **2013**, *187*, 40–44. DOI: 10.1016/j.snb.2012.09.022.

[7] Ascorbe, J.; Corres, J. M.; Arregui, F. J.; Matias, I. R. Recent Developments in Fiber Optics Humidity Sensors. *Sensors* **2017**, *17*, 893. DOI: 10.3390/s17040893.

[8] Zamarreno, C. R.; Hernaez, M.; Del Villar, I.; Matias, I. R.; F. J. Lossy, A. Mode Resonance-Based Optical Fiber Humidity Sensor. IEEE Sensors Conference, Limerick, Ireland, Oct 28–31. **2011.** pp. 234–237.

[9] Sanchez, P.; Zamarreño, C. R.; Hernaez, M.; Del Villar, I.; Fernandez-Valdivielso, C.; Matias, I. R.; Arregui, F. J. Lossy Mode Resonances toward the Fabrication of Optical Fiber Humidity Sensors. *Meas. Sci. Technol.* **2012**, *23*, 014002–014007. DOI: 10.1088/0957-0233/23/1/014002.

[10] Bogdanowicz, R.; Niedziałkowski, P.; Sobaszek, M.; Burnat, D.; Białobrzeska, W.; Cebula, Z.; Sezemsky, P.; Koba, M.; Stranak, V.; Ossowski, T.; Śmietana, M. Optical Detection of Ketoprofen by Its Electropolymerization on an Indium Tin Oxide-Coated Optical Fiber Probe. *Sensors* **2018**, *18*, 1361. DOI: 10.3390/s18051361.

[11] Hernaez, M.; Zamarreño, C. R.; Villar, I. D.; Arregui, F. J.; Matias, I. R. Optical Fiber Humidity Sensor Based on Lossy Mode Resonances. *Int. J. Smart Sens. Intell. Syst.* **2009**, *2*, 653–660. DOI: 10.21307/ijssis-2017-373.

[12] Zamarreño, C. R.; Hernaez, M.; Sanchez, I.; Del Villar, I.; Matias, I. R.; Arregui, F. J. Optical Fiber Humidity Sensor Based on Lossy Mode Resonances Supported by TiO_2/PSS Coatings. *Procedia Eng.* **2011**, *25*, 1385–1388. DOI: 10.1016/j.proeng.2011.12.342.

[13] Pedro, J.; Rivero, A.; Urrutia, J.; Goicoechea, F. J.; Arregui, F. J. Optical Fiber Humidity Sensors Based on Localized Surface Plasmon Resonance (LSPR) and Lossy-Mode Resonance (LMR) in Overlays Loaded with Silver Nanoparticles. *Sensors Actuat. B: Chem.* **2012**, *173*, 244–249. DOI: 10.1016/j.snb.2012.07.010.

[14] Razquin, L.; Zamarreno, C. R.; Munoz, F. J.; Matias, I. R.; Arregui, F. J. thrombin detection by Means of an Aptamer Based Sensitive Coating Fabricated onto LMR-Based Optical Fiber Refractometer, IEEE Sensors, Taipei, 2012. pp. 1–4. DOI: 10.1109/ICSENS.2012.6411186.

[15] Wang, Q.; Jian-Ying, J.; Bo-Tao, W. Highly Sensitive SPR Biosensor Based on Graphene Oxide and Staphylococcal Protein a Co-Modified TFBG for Human IgG Detection. *IEEE Trans. Instrum. Meas.* **2019**, DOI: 10.1109/TIM.2018.2875961.

[16] Wang, Q.; Jian-Ying, J.; Xue-Zhou, W.; Li-Ye, N.; Wan-Ming, Z. A D-Shaped Fiber Long-Range Surface Plasmon Resonance Sensor with High Quality Factor and Temperature Self-Compensation. *IEEE Trans. Instrum. Meas.* **2019**, DOI: 10.1109/TIM.2019.2920187.

[17] Zamarreno, C. R.; Hernaez, M.; Del Villar, I.; Matias, I. R.; Arregui, F. J. Tunable Humidity Sensor Based on ITO-Coated Optical Fiber. *Sensors Actuat. B: Chem.* **2010**, *146*, 414–417. DOI: 10.1016/j.snb.2010.02.029.

[18] Zamarreno, C. R.; Hernaez, M.; Del Villar, I.; Matias, I. R.; Arregui, F. J. Optical Fiber Biosensor Based on Lossy Mode Resonances. *Smart Sensors Meas. Instrum.* **2011**, *174*, 263–269.

[19] Elosúa, C.; Vidondo, I.; Arregui, F. J.; Bariain, C.; Luquin, A.; Laguna, M.; Matías, I. R. Lossy Mode Resonance Optical Fiber Sensor to Detect Organic Vapors. *Sensors Actuat. B: Chem.* **2013**, *187*, 65–71. DOI: 10.1016/j.snb.2012.09.046.

[20] Zamarreno, C. R.; Ardaiz, I.; Ruete, L.; Muñoz, F. J.; Matias, I. R.; Arregui, F. J. C-Reactive protein aptasensor for Early Sepsis Diagnosis by Means of an Optical Fiber Device. *Sensors, IEEE* **2013**, 1–4.

[21] Socorro, A. B.; Corres, J. M.; Del Villar, I.; Matias, I. R.; Arregui, F. J. Immunoglobulin g sensor by Means of Lossy Mode Resonances Induced by a Nanostructured Polymeric Thin-Film Deposited on a Tapered Optical Fiber. Trends in Nano Technology Conference, Madrid, Spain, **2012**.

[22] Gupta, B. D.; Usha, S. P.; Shrivastav, A. M. A Novel Approach of LMR/MIP for Optical Fiber Based Salivary Cortisol Sensor. *CLEO: Applications and Technology* **2016**, JTu5A.145.

[23] Socorro, A. B.; Corres, J. M.; Del Villar, I.; Matias, I. R.; Arregui, F. J. Celiac Disease Biodetection Using Lossy Mode Resonances Generated in Tapered Single-Mode Optical Fibers. 23rd Conference on Optical Fiber Sensors, Santander, Spain, **2014**; Vol. 9157. DOI: 10.1117/12.2059254.

[24] Del Villar, I.; Zamarreno, C. R.; Hernaez, M.; Arregui, F. J.; Matias, I. R. Lossy Mode Resonance Generation with Indium-Tin-Oxide-Coated Optical Fibers for Sensing Applications. *J. Lightwave Technol.* **2010**, *28*, 111–117. DOI: 10.1109/JLT.2009.2036580.

[25] Paliwal, N.; John, J. Theoretical Modeling of Lossy Mode Resonance Based Refractive Index Sensors with ITO/TiO_2 Bilayers. *Appl. Opt.* **2014**, *53*, 3241–3246. DOI: 10.1364/AO.53.003241.

[26] Socorro, A. B.; Del Villar, I.; Corres, J. M.; Arregui, F. J.; Matias, I. R. Spectral Width Reduction in lossy mode resonance-Based Sensors by Means of Tapered Optical Fibre Structures. *Sensors Actuat. B: Chem.* **2014**, *200*, (53–60. DOI: 10.1016/j.snb.2014.04.017.

[27] Zubiate, P.; Zamarreño, C. R.; Del Villar, I.; Matias, I. R.; Arregui, F. J. High Sensitive Refractometers Based on Lossy Mode Resonances (LMRs) Supported by Coated D-Shaped Optical Fibers. *Opt. Express* **2015**, *23*, 8045–8050. DOI: 10.1364/OE.23.008045.

[28] Del Villar, I.; Zamarreño, C. R.; Sanchez, P.; Hernaez, M.; Valdivielso, C. F.; Arregui, F. J.; Matias, I. R. Generation of Lossy Mode Resonances by Deposition of High-Refractive-Index Coatings on Uncladded Multimode Optical Fibers. *J. Opt.* **2010**, *12*, 095503. DOI: 10.1088/2040-8978/12/9/095503.

[29] Hernáez, M.; Del Villar, I.; Zamarreño, C. R.; Arregui, F. J.; Matias, I. R. Optical Fiber Refractometers Based on Lossy Mode Resonances Supported by TiO_2 Coatings. *Appl. Opt.* **2010**, *49*, 3980–3985. DOI: 10.1364/AO.49.003980.

[30] Paliwal, N.; John, J. Theoretical Modeling and Investigations of AZO Coated LMR Based Fiber Optic Tapered Tip Sensor Utilizing an Additional TiO_2 Layer for Sensitivity Enhancement. *Sensors Actuat. B: Chem.* **2017**, *238*, 1–8. DOI: 10.1016/j.snb.2016.07.032.

[31] Wang, Q.; Zhao, W.-M. Optical Methods of Antibiotic Residues Detections: A Comprehensive Review. *Sensors Actuat. B: Chem.* **2018**, *269*, 238–256. DOI: 10.1016/j.snb.2018.04.097.